Mutual dependence of oxygen and vacancy diffusion in bcc Fe and dilute iron alloys

X. Wang,[1,2] J. Faßbender,[1,2] and M. Posselt[1,*]

[1]*Helmholtz-Zentrum Dresden—Rossendorf, Institute of Ion Beam Physics and Materials Research, Bautzner Landstraße 400, 01328 Dresden, Germany*

[2]*Technische Universität Dresden, 01062 Dresden, Germany*

(Received 31 January 2020; revised manuscript received 20 March 2020; accepted 21 April 2020; published 13 May 2020)

A combination of density functional theory (DFT) and an efficient calculation method based on atomistic kinetic Monte Carlo simulations (AKMC) is used to investigate the interdependence of oxygen (O) and vacancy (v) diffusion in bcc Fe and in dilute iron alloys with the substitutional atoms Y and Ti. Both O and v are considered as mobile while the substitutional atoms are assumed to be immobile. DFT is applied to determine the binding energy between O and v for different distances, the migration barriers for O in the environment of v, and the corresponding barriers of v in the vicinity of O. In agreement with previous work O and v have a very strong binding at the first-neighbor distance. On the other hand, the calculations show that the Ov pair at the sixth-neighbor distance is instable. The simultaneous jumps of both O and v compensate the lack of jump paths that would occur due to this instability. The DFT results are employed to determine the diffusion coefficient of O and v using the AKMC-based calculation method. At first a model system with fixed O and v concentrations is studied. It is found that even a small v content of some parts per million can lead to a strong reduction of the O diffusivity. A similar effect is obtained for v diffusion under the influence of O. Furthermore, investigations on the interdependence of O and v diffusion in the first phase of thermal processing of oxide dispersion strengthened iron alloys are performed, and the influence of the substitutional atoms Y and Ti is studied. A simple thermodynamic model is employed to determine the concentration of O, Y, and Ti monomers as well as the total v concentration, for a typical total content of O, Y, and Ti. These results are used in calculations of the diffusion coefficients of O and v. Not only a strong mutual dependence but also a significant influence of Y on O diffusion is found. Finally, O and v diffusivities in a system with an O content close to the thermal solubility are calculated, where the monomer and total concentrations are determined by two different thermodynamic models. Even for such a low amount of O in the alloy the diffusion coefficients differ strongly from those in perfect bcc Fe.

DOI: 10.1103/PhysRevB.101.174107

I. INTRODUCTION

Materials properties are decisively influenced by diffusion processes. Very often diffusion cannot be avoided during fabrication and application. Therefore, many efforts were made to understand the underlying atomic-level mechanisms (see [1]). It was found that diffusion proceeds via interstitial sites if the size of the migrating atom is smaller than that of the host atoms. Foreign atoms with sizes similar to or larger than those of the host material diffuse via the vacancy or the interstitialcy mechanism. In this case vacancies and self-interstitials must be available. Since at thermal equilibrium the concentration of these point defects is very low, the migration via the vacancy and the interstitialcy mechanism is much slower than that via the interstitial sites.

Dilute iron-based ferritic alloys are used as structural materials for a plethora of applications. These alloys contain foreign atoms intentionally employed to improve certain properties as well as unwanted impurities introduced during manufacturing. The diffusion of a certain foreign atom may be influenced by other foreign atoms and intrinsic point defects. Recently, the authors of this work have investigated theoretically how the presence of substitutional atoms such as Al, Si, P, S, Ti, Cr, Mn, Ni, Y, Mo, and W affects the oxygen (O) diffusion in bcc Fe [2]. Depending on the interaction between oxygen and a foreign atom the influence on O diffusion may be strong or weak. For example, in the case of Ti, with a concentration of about 0.1 at. %, at 500 K the diffusion coefficient of oxygen is three orders of magnitudes lower than that in pure bcc Fe. On the other hand, at the same temperature and concentration, the influence of Si on oxygen diffusion is negligible. The most stable position of oxygen in bcc Fe is the octahedral interstitial site. In perfect bcc Fe as well as in a dilute alloy with substitutional atoms oxygen diffuses mainly via nearest-neighbor jumps between these sites [2]. Therefore, the oxygen diffusion is much faster than that of the substitutional foreign atoms so that these atoms were assumed to be immobile. However, if oxygen diffusion is investigated under the influence of vacancies, the vacancy mobility cannot

*Corresponding author: Helmholtz-Zentrum Dresden—Rossendorf, Bautzner Landstraße 400, 01328 Dresden, Germany; m.posselt@hzdr.de

be neglected, since the migration barrier in perfect bcc Fe is not much higher than that of oxygen.

Under conditions of thermal equilibrium, the oxygen as well as the vacancy concentration in pure bcc Fe is very small. However, Schuler *et al.* [3] demonstrated that even an oxygen concentration in the order of the thermal solubility limit may lead to a significant increase of the total vacancy (v) concentration. This is due to the strong attraction between O and v.

Due to the extremely low solubility of oxygen [4–8] the measurement of oxygen diffusion in iron is difficult. Only a few experimental data are available. They were obtained many years ago using the method of internal oxidation of solutes which have a higher affinity to oxygen than iron [4–9]. Frank *et al.* [9] performed a critical review of experimental data published before 1967 and derived a value for the diffusion activation energy. In 1967 Swisher and Turkdogan [5] determined the oxygen diffusion coefficient in bcc Fe from measurements at temperatures above about 970 K. In 1986 Takada *et al.* [6–8] published diffusion data obtained from experiments at temperatures between 1023 and 1173 K, i.e., mainly for the paramagnetic state of bcc Fe. The lack of experimental data directly obtained from an oxygen concentration profile in pure bcc Fe and for a sufficiently wide temperature range is an important motivation for theoretical investigations on oxygen diffusion, with the focus on a better understanding of the atomic-level mechanisms.

Barouh *et al.* [10] investigated by density functional yheory (DFT) calculations the mobility of clusters formed by the interstitial solutes carbon, nitrogen, and oxygen with vacancies. The main motivation for this work was the fact that these foreign atoms attract the vacancy, so that they may possibly migrate as pairs or clusters. In the oxygen case the attraction is much stronger than for C and N. Barouh *et al.* [10] found that the decisive migration barriers for the Ov pair and the O_2v cluster are higher than the barrier for the O monomer, whereas the relevant barrier for the Ov_3 cluster is similar to that for the monomer. That means that an extraordinarily high vacancy concentration is required to obtain an effective oxygen diffusion coefficient that is higher than in perfect iron. Shang *et al.* [11] used DFT to determine the migration barrier of oxygen in the vicinity of a vacancy and found that this barrier is much higher than in perfect Fe. This is in agreement with the results of Barouh *et al.* [10]. Furthermore, Shang *et al.* [11] claimed that their findings lead to a reasonable agreement with the measured oxygen diffusion coefficient [5–9]. However, this agreement could be only obtained since these authors assumed that every migration barrier of oxygen has a height as in the close environment of the vacancy. This does not correspond to reality, since the equilibrium concentration of vacancies in bcc Fe is very small, so that oxygen is mainly moving in pure iron where the migration barrier is much lower. Also the assumption of Shang *et al.* [11] that during O diffusion the position of the vacancy is fixed is not realistic (see above).

The focus of the present work is on the mutual dependence of oxygen and vacancy diffusion in bcc Fe and dilute iron alloys. DFT calculations are used to determine the binding energy between oxygen and the vacancy for different distances, and to obtain the migration barriers for oxygen in the environment of a vacancy and for the vacancy in the environment of an oxygen atom. Using the data determined by DFT as inputs for a recently developed efficient calculation method [12] that is based on atomistic kinetic Monte Carlo (AKMC) simulations, the simultaneous migration of O and v is considered. At first the diffusion coefficients of oxygen in a model system with fixed vacancy concentrations, the diffusion coefficients of the vacancy for fixed oxygen concentrations, and the diffusivity of the Ov pair are determined. In reality the vacancy and oxygen concentrations in dilute Fe-based alloys are determined by the thermal equilibrium with other foreign atoms and intrinsic defects or are affected by external conditions. Vacancy concentrations significantly above the equilibrium value in pure bcc Fe may occur due to irradiation, strong plastic deformation, mechanical alloying, etc. An example of the latter case is the production of oxide dispersion strengthened (ODS) Fe-based alloys using powder technology. In this work the oxygen and vacancy diffusion in the first stage of thermal processing of the ODS alloys is investigated using the DFT data for binding and migration energies. Since the initial powder contains not only relatively high concentrations of oxygen and vacancies but also Y and Ti, the influence of these most relevant substitutional solutes is also considered. In contrast to O and v the substitutional atoms Y and Ti can be assumed to be immobile. In the last part of the work O and v diffusion is studied for pure bcc Fe with an oxygen content close to the thermal solubility. The calculated diffusion coefficient of oxygen is compared with the few available experimental data.

II. DFT CALCULATIONS

A. Computational method

The calculations were performed within the framework of DFT as implemented in the Vienna *ab initio* simulation package (VASP) [13–15]. The VASP code uses pseudopotentials generated by the projector-augmented wave [16,17] approach. Exchange and correlation effects are described by the generalized gradient approximation with the Perdew-Burke-Ernzerhof parametrization [18]. In the calculations a supercell consisting of $4\times4\times4$ bcc unit cells was considered and a $3\times3\times3$ k point grid was employed for the Brillouin-zone sampling within the Monkhorst-Pack scheme [19]. For the integration in the reciprocal space the Methfessel-Paxton smearing method [20] was applied with a width of 0.2 eV. All calculations were carried out within the framework of the spin-polarized formalism and with a plane-wave cutoff energy of 500 eV. After introduction of foreign atoms or of a vacancy into the supercell, the position of atoms as well as the volume and shape of the supercell were relaxed so that the total stress/pressure of the supercell tends to zero. The convergence criteria were set to 10^{-2} eV/Å and 10^{-5} eV for the residual force per atom and the change of total energy in one iteration step, respectively. As shown in previous investigations [21–26], oxygen prefers the octahedral interstitial sites in bcc Fe, and the most stable site for vacancy is the bcc lattice site.

Figure 1(a) [Fig. 1(b)] illustrates the neighboring octahedral interstitial (substitutional) sites of a vacancy (oxygen) up

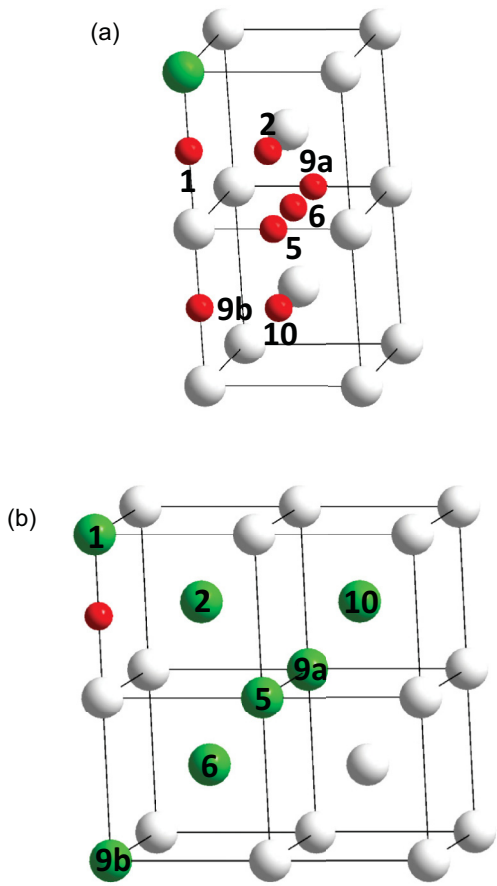

FIG. 1. (a) Examples for octahedral interstitial sites of oxygen (red) in the neighborhood of a vacancy (green). Neighbors inside the interaction region considered in DFT calculations are marked by black numbers. The gray spheres represent Fe atoms. (b) Examples for bcc sites of the vacancy (green) in the neighborhood of an oxygen atom (red). The meaning of the black numbers is the same as in (a).

to the tenth-neighbor position. The notation and numbering of the neighbor positions is according to the scheme for the underlying simple cubic lattice (see [2,10]) which consists of bcc lattice sites and all octahedral interstitial sites of the bcc lattice. Within this scheme oxygen cannot reside on third-neighbor, fourth-neighbor, seventh-neighbor, eighth-neighbor, etc., positions of the vacancy since these sites are already occupied by iron atoms. Furthermore, there are two different ninth-neighbor sites (9a and 9b).

The binding energy of an oxygen-vacancy (Ov) pair at a certain distance is determined by

$$E_{\text{bind}} = E(\text{Ov}) + E_0 - E(\text{v}) - E(\text{O}), \tag{1}$$

with E_0 as the total energy of the perfect bcc Fe supercell. $E(\text{Ov})$, $E(\text{v})$, and $E(\text{O})$ denote the total energy of the supercell with the Ov pair, with a single vacancy, and a single oxygen atom, respectively. Negative values of the binding energy mean that the interaction is attractive.

The minimum energy paths and the respective migration barriers were calculated using the standard nudged elastic band (NEB) method [27,28] and, subsequently, the climbing-image NEB method [29]. For comparison, also the solid-state NEB [30] was employed in some cases. The results do not differ significantly from those obtained by the combination of standard NEB and climbing-image NEB. For all these calculations the VTSTTOOLS [31] provided by the Henkelman group at the University of Texas (Austin) were used.

The diffusion coefficient of the interstitial oxygen atom or of the vacancy in perfect bcc Fe may be obtained from the general formula [32]

$$D = \frac{n_p \nu l^2}{2d}, \tag{2}$$

with the jump rate ν, jump length l, and the dimension of the diffusion d, as well as the number of possible equivalent jumps n_p of the diffusing atom (or vacancy) from a given position. In the case of oxygen diffusion via jumps between nearest-neighbor octahedral interstitial sites, the quantities n_p, d, and l are given by

$$n_p = 4, \quad d = 3, \quad l = a/2 \ (a\text{: lattice constant of bcc Fe}), \tag{3}$$

while for the diffusion of the vacancy one obtains

$$n_p = 8, \quad d = 3, \quad l = \frac{\sqrt{3}}{2}a. \tag{4}$$

In general, the jump rate is given by

$$\nu = \nu_0 \exp\left(-\frac{E_m}{k_B T}\right), \tag{5}$$

with the migration barrier E_m, the Boltzmann constant k_B, and the temperature T. In the high-temperature limit, which is valid in all cases considered in this work, the attempt frequency ν_0 is determined by the Vineyard formula [33]:

$$\nu_0 = \frac{\prod_{i=1}^{3N-3} \nu_{\text{min},i}}{\prod_{i=1}^{3N-4} \nu_{\text{SP},i}}, \tag{6}$$

where $\nu_{\text{min},i}$ and $\nu_{\text{SP},i}$ are the vibrational frequencies of the supercell with the diffusing oxygen (or vacancy) at the saddle point (SP) and at an equilibrium (minimum) position, respectively. These frequencies were calculated using the method implemented in the VASP code which employs the harmonic approximation and the frozen phonon approach (see [26,34–36]).

B. Binding energy of oxygen-vacancy pairs at different distances

The binding energies of the Ov pair up to the tenth-neighbor distance are summarized in Table I. The most attractive state is found for the first-neighbor distance, and the attraction is still appreciable at the second-neighbor distance. With increasing distance, the interaction becomes weaker. Most of the binding energy data determined in the present work are consistent with previous DFT results [10,11,21–23,25].

A peculiarity was found for O and v at the sixth-neighbor distance. This state is not stable; i.e., during relaxation calculation the vacancy moves to the first-neighbor distance with respect to O. This result could be also reproduced with supercells containing 3×3×3 and 5×5×5 bcc unit cells and

TABLE I. Binding energy of the Ov pair at different distances between O and v (see Fig. 1). In this work the pair at the sixth-neighbor distance was found to be not stable; i.e., the vacancy relaxes to the first-neighbor distance with respect to O. The value with the asterisk (−0.34 eV) corresponds to the binding energy at a transition state which was found during the relaxation calculations (see text). DFT data from the literature are also given.

Neighbor position	1	2	5	6	9a	9b	10
E_{bind} (eV)	−1.596	−0.697	−0.126	−0.34*	0.019	0.138	0.015
	−1.52 [10]	−0.58 [10]	−0.05 [10]	−0.35 [10]	0.01 [25]	0.22 [25]	
	−1.53 [11]	−0.65 [11]	−0.08 [11]	−0.37 [23]			
	−1.45 [21]	−0.60 [21]	−0.14 [23]				
	−1.65 [22]	−0.75 [22]					
	−1.69 [23]	−0.73 [23]					

in a calculation with a higher precision (convergence criteria 10^{-4} eV/Å and 10^{-9} eV for force and energy change, respectively) for a supercell with 4×4×4 unit cells. For a supercell with 4×4×4 bcc unit cells relaxation calculations at constant volume were also performed, and the result was very similar to that obtained by the other calculations. The relaxation process was studied in more detail, and it was found that before completely relaxing to the first-neighbor distance a transition state of the Ov pair can be identified. For this nonstable state a "quasi-binding energy" of about −0.34 eV could be estimated. This value is very similar to that obtained in previous DFT calculations (−0.37 eV [23], −0.35 eV [10]) for the binding energy of the Ov pair at the sixth-neighbor distance. In contrast to the result of this work these authors consider the Ov pair at the sixth-neighbor distance as (meta)stable. On the other hand, Barouh *et al.* [10] found that the migration barrier for the vacancy jump from the sixth- to the first-neighbor distance is 0, which is in accord with the result of the present work, showing that the Ov pair at the sixth-neighbor distance is not really stable.

From previous DFT calculations it is known that the incorporation of an oxygen atom on an octahedral interstitial site of the bcc Fe lattice leads to considerable tetragonal distortion, whereas the distortion due to the first-neighbor Ov pair is much smaller (see [26]). In the present work tetragonal distortions are also found for first-, second-, and ninth-neighbor Ov pairs. The instability of the sixth-neighbor pair could be explained by the fact that such an atomic configuration causes very strong distortions, leading to an immediate relaxation towards the first-neighbor pair.

C. Migration barriers

1. Oxygen and vacancy migration in pure bcc Fe

The diffusion of oxygen in perfect bcc Fe was investigated by several authors. It was found that oxygen migrates via nearest octahedral interstitial sites with a tetrahedral site as saddle point. The following jump barriers were obtained: 0.512 eV [2], 0.56 eV [10], 0.526 eV [11], 0.60 eV [21], 0.48 eV [23], and 0.451 eV [37]. Furthermore, for the oxygen atom attempt frequencies of 15.76 THz [2] and of about 13 THz [11] were determined.

Vacancy migration from one bcc site to the nearest-neighbor bcc site corresponds to a jump of a Fe atom in the opposite direction. NEB calculations showed that the minimum energy path is a straight line with a migration barrier of 0.695 eV. This value is in good agreement with previous DFT results (0.68 eV [26], 0.64 eV [34], 0.65 eV [38], 0.67 eV [39], 0.68 eV [40], 0.66 eV [41], and 0.67 eV [42]). The saddle point of the nearest-neighbor vacancy jump corresponds to the atomic configuration with the jumping Fe atom in the middle between the original and the final site of the vacancy. It should be noticed that the jump distance of the vacancy corresponds to a third-neighbor distance in the underlying simple cubic lattice (see Sec. II A). Using the calculation method described in Sec. II A, an attempt frequency of 15.33 THz was obtained for the vacancy jump in pure bcc Fe. This value is comparable with the result (11.6 THz) of recent DFT calculations [43]. Investigations of vacancy jumps over second- and third-neighbor distances of the bcc lattice showed that in pure bcc Fe these long-distance jumps consist of successive nearest-neighbor jumps between bcc lattice sites. It is worth mentioning that different Fe atoms take part in these successive nearest-neighbor jumps of the vacancy.

Since the migration barriers of O (0.512 eV) and v (0.695 eV) are in the same order of magnitude, the mobility of both species must be considered in order to determine the diffusion coefficient of oxygen in bcc Fe in the presence of a vacancy and to calculate the diffusion coefficient of the vacancy in the presence of oxygen. This is different from previous investigations [2] on the influence of substitutional foreign atoms on the migration of oxygen, with O as the only mobile species.

2. Vacancy influence on oxygen migration barriers, and oxygen influence on vacancy migration barriers

(a) Cage jumps of oxygen. Since the presence of a vacancy is related to additional free volume, the oxygen atom can jump from one nearest-neighbor site with respect to the vacancy to another. The corresponding jump length is the second-neighbor distance between octahedral interstitial sites. This process is called cage jump [10] and is illustrated in Fig. 2. A barrier height of 0.576 eV was obtained from NEB calculations. Barouh *et al.* [10] got a lower value (0.40 eV) which might be explained by the fact that they used the DFT code SIESTA and the drag method to determine migration barriers. The value of 0.576 eV is slightly higher than that for the first-neighbor jump of oxygen in pure Fe (0.512 eV, see Sec. II C 1), but considerably lower compared to barriers which must be overcome by O and v to escape the state of

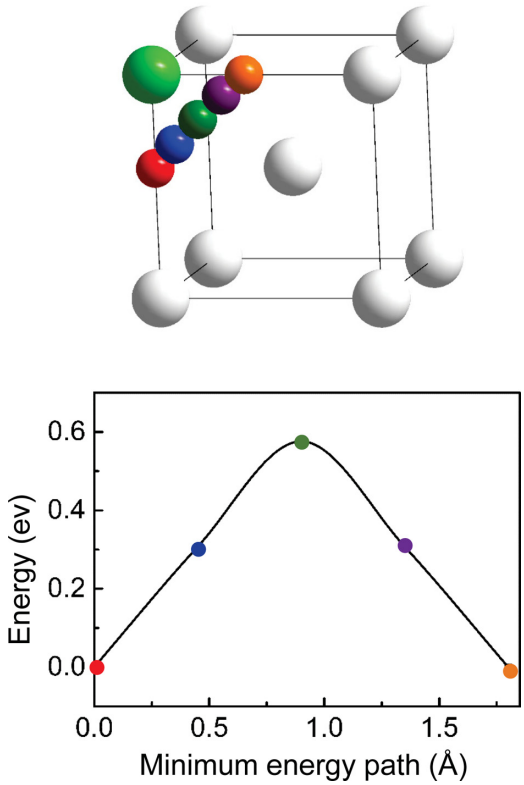

FIG. 2. Minimum energy path of the cage jump of oxygen. The large green sphere represents the vacancy.

the nearest-neighbor Ov pair (see below). Therefore, the cage jump is the most probable jump once oxygen and vacancy are trapped at this strong attractive state. However, as already pointed out by Barouh *et al.* [10] the cage jump of oxygen around the first-neighbor vacancy does not really contribute to net diffusion of oxygen, the vacancy, and the oxygen-vacancy pair.

(b) Nearest-neighbor O and v jumps as well as simultaneous jumps of O and v. In order to calculate the possible migration barriers by the NEB method two cases were considered: (i) oxygen jumps if the vacancy position is fixed, and (ii) vacancy jumps if the oxygen position is fixed. The connectivity plot depicted in Fig. 3(a) illustrates all potential jumps of O and v within the interaction region, i.e., up to the tenth-neighbor distance. The dotted and dashed lines mark jumps that are not possible in reality, due to the instability of the Ov pair at the sixth-neighbor distance (see above) and because of the problem with the vacancy jump between states 2 and 5 (see below), respectively.

Figure 3(b) shows the barriers for oxygen jumps between nearest-neighbor octahedral sites, in the neighborhood of the vacancy (1-2, 2-5, 5-10, and 9b-10), as well as the barrier for the cage jump. The values for the O jumps from 1 to 2 and 2 to 1 as well as from 2 to 5 and 5 to 2 are consistent with results of Barouh *et al.* [10]. The data for vacancy jumps between nearest-neighbor bcc lattice sites, in the neighborhood of oxygen (1-2, 2-9a, 5-10, 9a-10), are also given in Fig. 3(b). As already mentioned, in the present work migration barriers were determined up to the tenth-neighbor distance. It is assumed that at larger distances the interaction between O

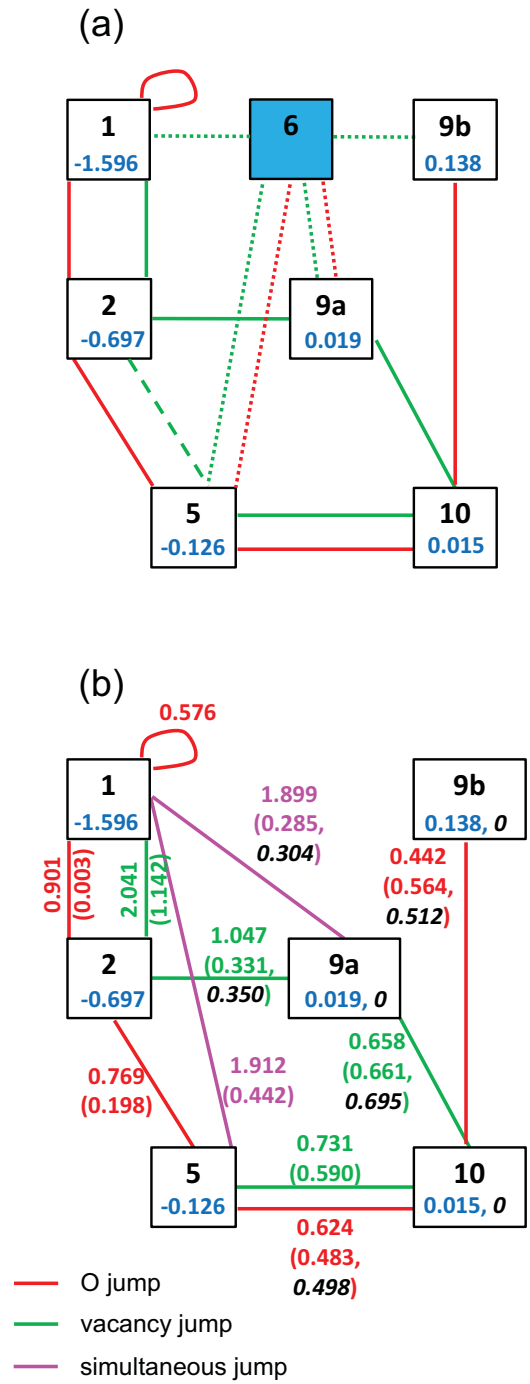

FIG. 3. Graphical representation of possible jumps of oxygen and the vacancy between different neighbor positions (connectivity plots). Potential jumps (O: red; v: green) including the sixth-neighbor position are depicted in (a). However, the instability of the Ov pair at the sixth-neighbor distance makes jumps marked by dotted lines impossible. For other reasons (see text) the direct vacancy jump marked by the dashed line is not possible. (b) illustrates the really relevant neighbor positions and jumps. Jump barriers for forward and backward jumps are given in eV, e.g., for oxygen jump from 2 to 5 the barrier is 0.769 eV, while it is 0.198 eV for the jump from 5 to 2. In both figures the binding energy of the Ov pair at a given distance is marked by blue color. The black italic numbers in (b) show the binding energies and migration barriers modified due to the rule of detailed balance (see text).

and v is negligible so that in this region the migration energies of both species correspond to that in pure bcc Fe.

If the Ov pair at the sixth-neighbor distance were stable, both O and v could jump between the fifth and the sixth neighbor as well as between the neighbors 9a and 6; see Fig. 3(a). These two cases are worth investigating in more detail. Due to the instability of the Ov pair at the sixth-neighbor distance the attempt of an oxygen jump from 5 towards 6 causes a simultaneous (or coupled) vacancy jump so that finally both species are at the first-neighbor distance. NEB calculations yield a barrier of 0.442 eV for such a simultaneous jump of both O and v. Figure 4 shows the initial, intermediate, and final atomic configurations for this case. The opposite jump has a much higher barrier (1.912 eV). Also the attempt of an oxygen jump from 9a towards 6 leads to a simultaneous v jump which results in a final configuration with both species at the first-neighbor distance. The barrier of this simultaneous jump is 0.285 eV, and the initial, intermediate, and final atomic configurations are also depicted in Fig. 4. The barrier for the opposite jump is 1.899 eV. It is interesting that in the cases illustrated in Fig. 4 the relatively high barriers for the jumps between 1 and 5 as well as between 1 and 9a are comparable with the barrier for the jump of the vacancy from the first to the second neighbor of O [Fig. 3(b)], and these barriers are somewhat higher than the combination of successive jumps of O from 1 to 2 and from 2 to 5 (1.667 eV). The two simultaneous jumps of Fig. 4 are marked by magenta color in the connectivity plot depicted in Fig. 3(b).

A barrier for the direct vacancy jump between the second and the fifth neighbor of O could be not determined by the NEB method due to lacking convergence. Therefore, these jumps are not considered in the present work. It might be possible that Barouh *et al.* [10] faced a similar problem, since they did not show results for those jumps. Obviously, the difficulty to determine the above-mentioned barriers is caused by the negligible barrier (0.003 eV) for the O jump between the second and the first neighbor of v: If v attempts to jump from the second to the fifth neighbor of O, at first the oxygen atom may migrate to the first-neighbor octahedral interstitial site of v. Then, the first simultaneous jump mechanism as described above may occur, i.e., O and v are initially at the first-neighbor distance, and finally at the fifth-neighbor distance. These assumptions are supported by the fact that the (not fully convergent) NEB calculations for the direct vacancy jump between the second and the fifth neighbor of oxygen yield a local minimum with an atomic configuration and a binding energy which correspond to O at the first-neighbor site of the v.

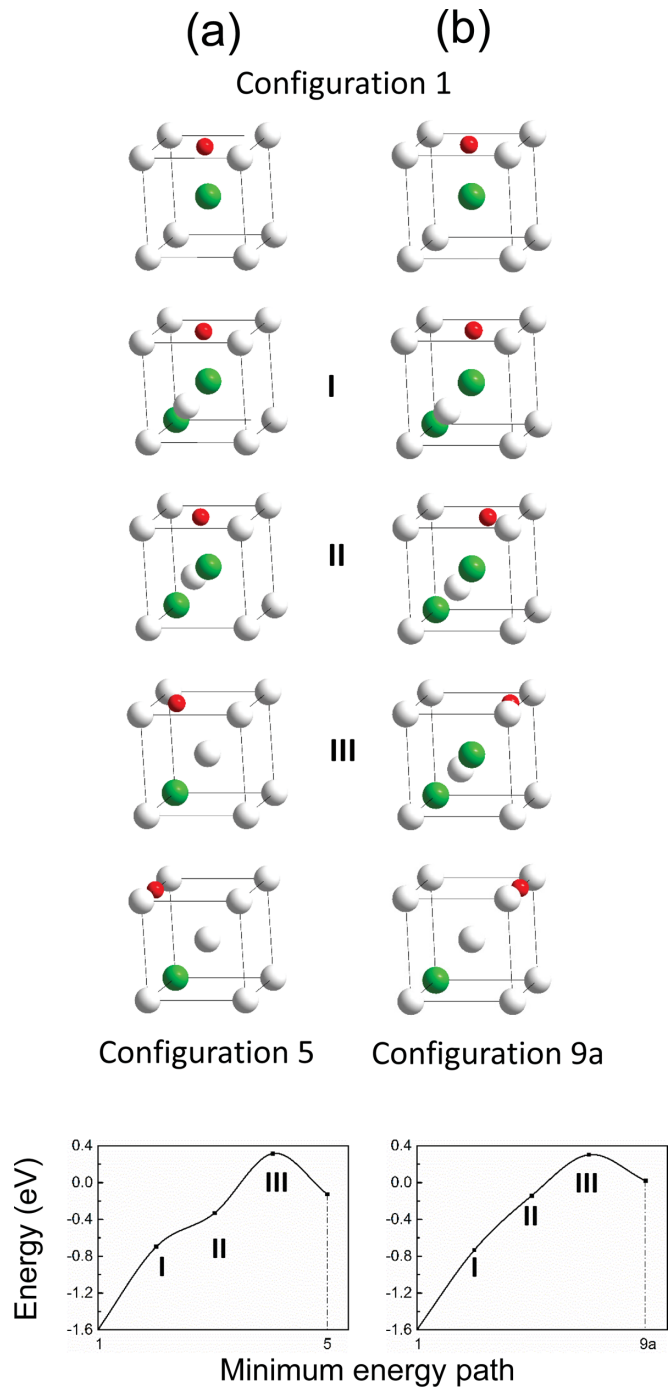

FIG. 4. Atomic configurations illustrating the simultaneous (or coupled) jumps between the first- and the fifth-neighbor position (a) and between the neighbor positions 1 and 9a (b). The scale on the ordinate concerns the binding energy of the Ov pair (see Table I).

III. AKMC BASICS AND DETERMINATION OF DIFFUSION COEFFICIENTS IN A MODEL SYSTEM

In order to use the NEB data for migration barriers in AKMC simulations in a consistent manner, the rule of detailed balance must be obeyed:

$$E_m^{i,j} - E_m^{j,i} = E_{\text{bind}}^{j} - E_{\text{bind}}^{i} \tag{7}$$

(see, e.g., [2]) for all the O and v jumps shown in the connectivity plot of Fig. 3(b). E_{bind}^{k} and $E_m^{k,l}$ are the binding energy between O and v at the kth-neighbor distance and the migration barrier for the jump between the kth and lth-neighbor distance, respectively. In present AKMC simulations the binding energy of the Ov pair at and beyond the ninth-neighbor distance was set to zero and in these regions the migration energy of O and v was set to the corresponding values in pure bcc Fe. Therefore, some of the NEB barriers at the rim of the interaction region had to be modified using Eq. (7). The modified data are also shown in Fig. 3(b).

In AKMC simulations a rigid lattice consisting of bcc lattice sites and octahedral interstitial sites is used. Therefore, the simultaneous (or coupled) jumps must be described in an approximate manner. In the case shown in Fig. 4(a), in the forward direction v jumps from the first- to the sixth-neighbor position (barrier 1.912) eV); afterwards O is simply shifted to the fifth-neighbor position of v. In the opposite direction O jumps from the fifth- to the sixth-neighbor position of v (barrier 0.442 eV); then v is shifted to the first-neighbor position of O. The jump depicted in Fig. 4(b) is also modeled in two steps. In one direction v jumps to the sixth-neighbor distance (barrier 1.899 eV) followed by the shift of O to the neighbor position 9a. In the other direction, O jumps to the sixth- neighbor distance (barrier 0.304 eV, correction due to detailed balance), followed by a shift of v to the first-neighbor distance of O.

The AKMC simulations used in this work are based on the residence time algorithm. Details of the calculation procedure were described in previous papers [2,12]. However, in the present work not only oxygen but also the vacancy is considered as mobile. In Ref. [12] an efficient method was developed to determine the diffusion coefficient of oxygen in bcc Fe under the influence of a low concentration of foreign atoms at the substitutional site. Such a procedure is also used in this work. In the following two subsections a model system with fixed vacancy or oxygen concentrations is considered in order to demonstrate the effect of vacancies on O diffusion and the influence of oxygen on v diffusion. In Secs. IV and V more realistic examples are studied.

A. Diffusion coefficient of oxygen in the presence of vacancies

For a given temperature and a given (sufficiently low) concentration of vacancies the diffusion coefficient of O can be determined by [12]

$$D = \frac{t_{\text{free}}}{t_{\text{total}}} D_{\text{free}} + \frac{t_{\text{inter}}}{t_{\text{total}}} D_{\text{inter}}, \tag{8a}$$

with

$$t_{\text{total}} = t_{\text{free}} + t_{\text{inter}} \tag{8b}$$

(see also Supplemental Material [44]).

The first and second terms are related to the diffusion of oxygen in perfect bcc Fe and within the region of interaction between oxygen and a vacancy, respectively. D_{free} denotes the diffusivity of oxygen in pure Fe, and D_{inter} denotes the diffusivity of oxygen in the interaction region. As already mentioned in Sec. II A the value of D_{free} can be obtained by the analytical expression

$$D_{\text{free}} = \frac{a^2}{6} \nu_0^{\text{free}} \exp\left(\frac{-E_m^{\text{free}}}{k_B T}\right), \tag{9}$$

with the attempt frequency $\nu_0^{\text{free}} = 15.76\,\text{THz}$ and the migration barrier $E_m^{\text{free}} = 0.512\,\text{eV}$, while $a = 2.832\,\text{Å}$ is the lattice constant in bcc Fe. The diffusion coefficient D_{inter} must be determined by AKMC simulations taking into account that O as well as v are mobile. In the dilute limit, which is considered throughout the present work for the concentrations of species that influence O (or v) diffusion, D_{inter} is nearly independent of the concentration of these species, i.e., nearly independent of the size of the AKMC simulations cell; see Ref. [12]. Therefore, D_{inter} can be determined by AKMC calculations for only one specific v concentration. In the interaction region the jumps are simulated using the attempt frequencies ν_0^{free} for O and v (see Sec. II C 1) and barriers according to Fig. 3(b). The quantities t_{free} and t_{inter} denote the sum of the time periods for diffusion outside and inside the interaction region, respectively, and t_{total} is the total diffusion time.

The time ratios in Eq. (8a) are given by the analytical expressions [12],

$$\frac{t_{\text{free}}}{t_{\text{total}}} = \frac{1 - \sum_i N_i C_{\text{v}}}{1 - \sum_i N_i C_{\text{v}} + \sum_i N_i \exp\left(-\frac{E^i_{\text{bind}}(\text{Ov})}{k_B T}\right) C_{\text{v}}} \quad i = 1, 2, 5, \tag{10a}$$

$$\frac{t_{\text{inter}}}{t_{\text{total}}} = \frac{\sum_i N_i \exp\left(-\frac{E^i_{\text{bind}}(\text{Ov})}{k_B T}\right) C_{\text{v}}}{1 - \sum_i N_i C_{\text{v}} + \sum_i N_i \exp\left(-\frac{E^i_{\text{bind}}(\text{Ov})}{k_B T}\right) C_{\text{v}}}, \quad (N_1 = 2,\ N_2 = 4,\ N_5 = 8), \tag{10b}$$

with the vacancy concentration C_{v}, and the binding energy $E^i_{\text{bind}}(\text{Ov})$ of the Ov pair at the ith-neighbor distance (see Table I, neighbor denotation according to Fig. 1); N_i is the number of possible vacancy sites at the ith-neighbor distance from O. Here neighbors beyond $i = 5$ are not taken into account because of the low binding energy. Note that in the dilute limit $\sum_i N_i C_{\text{v}}$ is small compared to $\sum_i N_i \exp(-\frac{E^i_{\text{bind}}(\text{Ov})}{k_B T}) C_{\text{v}}$.

At this point it must be emphasized that the use of Eqs. (8)–(10) to calculate the diffusion coefficient D for different vacancy concentrations is much more efficient than performing separate AKMC calculations for each concentration using simulation cells with different sizes. The method outlined above requires only one AKMC simulation to determine D_{inter} and in the remaining calculations one can employ analytical expressions for D_{free} and the time ratios. In this work D_{inter} was obtained by AKMC simulations for a vacancy concentration of 0.0977 at. %, i.e., using a simulation box consisting of 8 × 8 × 8 bcc unit cells with one mobile O atom and one mobile vacancy. In the Arrhenius plot $D_{\text{inter}}(T)$ is almost a straight line, from which the effective activation energy of about 2.0 eV was derived. The time ratios $t_{\text{free}}/t_{\text{total}}$ and $t_{\text{inter}}/t_{\text{total}}$ are depicted in Fig. 5, for vacancy concentrations of 0.0015, 0.0122, 0.0977, 0.2315, 0.4000, and 0.7813 at. %. With increasing temperature, $t_{\text{inter}}/t_{\text{total}}$ decreases while $t_{\text{free}}/t_{\text{total}}$ increases. Due to the strong attraction, in particular at the first-neighbor distance, the quantity $t_{\text{free}}/t_{\text{total}}$ rapidly decreases if the vacancy concentration increases. For concentrations above 0.0977% $t_{\text{free}}/t_{\text{total}}$ is nearly zero and $t_{\text{inter}}/t_{\text{total}}$ is nearly 1, even at elevated temperatures. At low temperature $t_{\text{free}}/t_{\text{total}}$ converges to zero and $t_{\text{inter}}/t_{\text{total}}$ approaches 1.

Figure 6(a) illustrates the total diffusion coefficient of oxygen in bcc Fe in dependence on the vacancy concentration. The data of D are between the values of the diffusion coefficient of oxygen in pure Fe (D_{free}) and that inside the region influenced by the vacancy (D_{inter}). The presence of vacancies significantly decreases the mobility of oxygen. For example, at 800 K and a concentration of 0.0015 at. % the diffusion

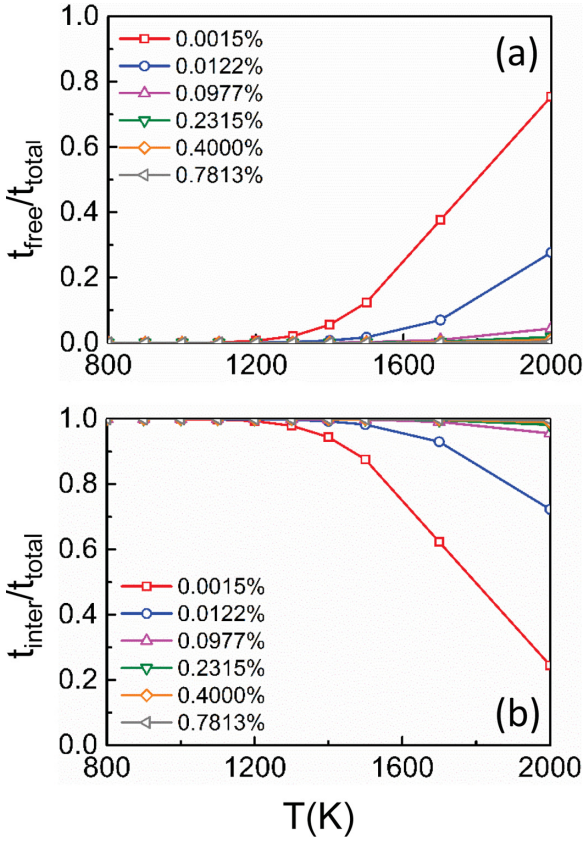

FIG. 5. The time ratios t_{free}/t_{total} (a) and t_{inter}/t_{total} (b) for oxygen, in dependence on temperature and vacancy concentration.

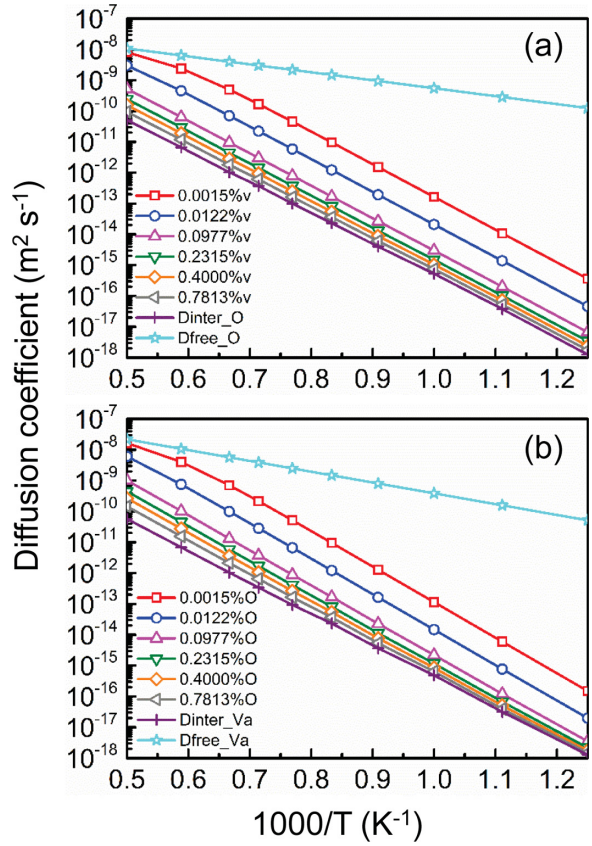

FIG. 6. The total diffusion coefficient of oxygen (a) for given concentrations of vacancies, and the total diffusion coefficient of the vacancy (b) for different oxygen concentrations. The corresponding data of D_{free} (cyan) and D_{inter} (violet) are also shown.

coefficient is five to six orders of magnitude lower than that in pure bcc Fe. With increasing vacancy concentration the reduction of D becomes slower and the value approaches that of D_{inter}.This is mainly due to the quick decrease of t_{free}/t_{total} with increasing v concentration. Note that in this work temperatures below 800 K were not considered, since in these cases AKMC simulations require extremely long computing times.

The total diffusion coefficient D can be also determined by

$$D = \frac{t_{free}}{t_{total}} D_{free} \tag{11}$$

if the interaction part $\frac{t_{inter}}{t_{total}} D_{inter}$ is negligibly small compared to $\frac{t_{free}}{t_{total}} D_{free}$ [see Eq. (8a)]. It is found that at concentrations of 0.0015, 0.0122, and 0.0977 at. % the total diffusion coefficient can be well reproduced by Eq. (11). At higher vacancy concentrations results obtained by (11) deviate from those determined by Eq. (8a). This is due to the fact that in these cases both terms of Eq. (8a) must be taken into account; their absolute values are very small but comparable.

The method described above may also be called the cluster expansion approach of diffusion. In the present case an Ov pair is temporarily formed during O migration. In our previous work [2,12] the temporary formation of pairs consisting of O and substitutional solutes was considered. In Secs. IV and V the method is extended to further applications (see also Supplemental Material [44]). A similar but more general approach which is based on the self-consistent mean field approach was recently developed by other authors [45–47].

B. Diffusion coefficient of the vacancy in the presence of oxygen

The method used in the last section to evaluate the diffusion coefficient of oxygen is also applied to study vacancy diffusion. The data for the diffusion coefficient of v in the interaction region with O (D_{inter}) were determined by AKMC simulations in a similar manner as D_{inter} for oxygen. Within the statistical accuracy of the AKMC data D_{inter} for v is nearly equal to D_{inter} for O, with an effective activation energy of about 2.0 eV. The time ratios t_{free}/t_{total} and t_{inter}/t_{total} used in the determination of the vacancy diffusion coefficient are calculated in a similar manner as in the case of the oxygen diffusion coefficient. The value of D_{free} for the vacancy is given by

$$D_{free} = a^2 \nu_0^{free} \exp\left(\frac{-E_m^{free}}{k_B T}\right), \tag{12}$$

with $E_m^{free} = 0.695$ eV and $\nu_0^{free} = 15.33$ THz (see Sec. II A). Considering both v and O jumps, AKMC simulations are performed in order to determine the diffusion coefficient of v in the interaction region with O. The total diffusion coefficient of the vacancy is illustrated in Fig. 6(b) for oxygen

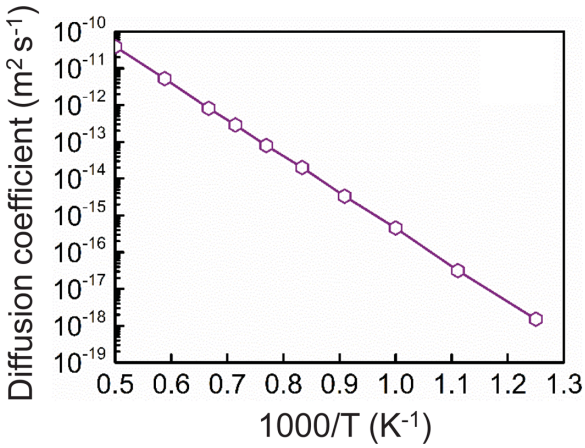

FIG. 7. Diffusion coefficient of the Ov pair inside the interaction region, determined by AKMC simulations, with one mobile oxygen and one mobile vacancy.

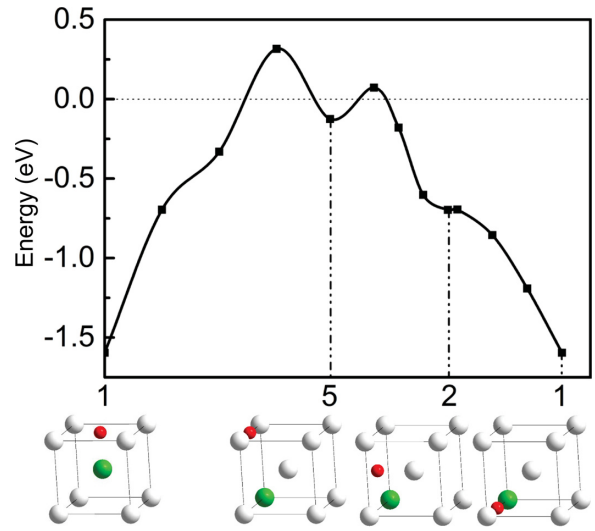

FIG. 8. Minimum energy path for the migration of the Ov pair. The scale concerns the binding energy of the Ov pair (see Table I).

concentrations of 0.0015, 0.0122, 0.0977, 0.2315, 0.4000, and 0.7813 at. %. The slope of these curves is slightly steeper than that of the curves for O [Fig. 6(a)] because of the somewhat steeper slope of D_{free} for the vacancy. The influence of O on the v diffusion coefficient is comparable with the influence of v on O diffusion: At 800 K and an oxygen concentration of 0.0015 at. % the diffusion coefficient is about five to six orders of magnitude lower than that in pure bcc Fe.

All the data presented in this work are strictly valid for ferromagnetic iron, i.e., below the Curie temperature of 1043 K. The temperature dependence of the spontaneous magnetization is not taken into account in the calculation of the basic DFT data (binding and migration energy); i.e., for bcc iron the ground-state value of magnetization is always assumed. Furthermore, above about 1183 K the fcc phase is most stable, and not bcc Fe. On the other hand, in this work temperatures up to 2000 K are considered in order to verify that the total diffusion coefficient of oxygen and of the vacancy (see Fig. 6) approaches the corresponding values for pure bcc Fe at sufficiently high temperature, and in order to study the hypothetical high-temperature behavior of other quantities.

C. Diffusion coefficient of the oxygen-vacancy pair

In AKMC simulations the position of the Ov pair is defined as the middle point between oxygen and vacancy. The calculation of the diffusion coefficient of the Ov pair is very similar to the determination of D_{inter} for O and v. Figure 7 depicts the result. The activation energy for Ov migration is about 1.95 eV, i.e., only slightly smaller than the activation energies found for D_{inter} of O and v (see above). This value may be the result of a simultaneous jump from first- to fifth-neighbor position, followed by an oxygen jump from the fifth- to the second-neighbor position [see Fig. 3(b)]. Finally, O jumps to the first-neighbor position of v with a negligible barrier of 0.003 eV. During this process the Ov pair has moved by a distance of a first-neighbor distance in bcc Fe (or a third-neighbor distance in the underlying simple cubic lattice; see Sec. II A). The most probable minimum energy path for the migration of the Ov pair is illustrated in detail in Fig. 8. The scale in Fig. 8 concerns the binding energy of the Ov pair. The difference between the lowest value (about −1.6 eV; see also Table I) and the highest value gives about 1.95 eV, i.e., the activation energy extracted from Fig. 7 for Ov pair migration. The present results are also in good agreement with the global migration energy of 1.90 eV determined by Barouh *et al.* [10] for the Ov pair. The dissociation energy of the Ov pair calculated by the sum of the absolute value of the first-neighbor binding energy and the oxygen migration energy in pure bcc Fe is about 2.11 eV which is 0.16 eV higher than the activation energy of pair migration. This estimation shows that pair migration is more probable than dissociation.

IV. OXYGEN AND VACANCY DIFFUSION IN THE FIRST STAGE OF THERMAL PROCESSING OF OXIDE DISPERSION STRENGTHENED Fe-BASED ALLOYS

In the calculation of the data shown in Figs. 5–7 constant vacancy and oxygen concentrations are assumed which are still rather low, but much higher than in pure bcc Fe at the thermal equilibrium [3,6–9]. A supersaturation of vacancies can occur under extreme conditions, e.g., under irradiation, plastic deformation, and mechanical alloying. The latter method is employed in the production of oxide dispersion strengthened (ODS) Fe-based alloys using powder technology. These materials are considered as promising candidates for structural materials of future fusion and fission reactors [48]. The mechanical alloying or milling process produces a lot of empty volume which may be considered as an additional source of vacancies. Furthermore, it is generally supposed that milling of a mixture containing a Fe-based alloy as well as Ti and Y_2O_3 leads to a nearly complete dissolution of yttria (Y_2O_3) [49,50]. Typical total O, Y, and Ti concentrations ($C_{\text{O}}^{\text{total}}$, $C_{\text{Y}}^{\text{total}}$, $C_{\text{Ti}}^{\text{total}}$) are 0.18, 0.12, and 1.05 at. %, respectively (for MA957

alloy see [49–51]). These data are used in the following considerations. Note that C_O^{total} is much higher than the thermal solubility of oxygen in bcc Fe. The strong attraction between oxygen and the vacancy, between O and Y, and between Y and the vacancy (see below) is assumed to be decisive for the high oxygen and Y incorporation ability of the ODS Fe-based alloys. The thermal processing of the ODS alloy is a complex and time consuming process which includes hot isostatic pressing or hot extrusion, and additional annealing (see, e.g., [52–56]). In the following the thermal treatment is described in a very simple manner by assuming equilibrium between O, Y, Ti, and vacancy monomers on the one hand and Ov, vY, vTi, OY, and OTi pairs on the other hand. This may correspond to the first phase of the thermal processing, i.e., to the beginning of the formation of the characteristic ODS clusters which contain O, v, Y and Ti. Any mechanical effects such as pressure and deformation are neglected in these considerations.

If only the most stable pairs,

- Ov at first-neighbor distance ($E_{bind} = -1.596$ eV), and at second-neighbor distance (-0.697 eV),
- OY at second-neighbor distance (-1.01 eV [2]), and at fifth-neighbor distance (-0.336 eV [2]),
- OTi at first-neighbor distance (-0.372 eV [2]), and at second-neighbor distance (-0.593 eV [2]),
- vY at third-neighbor distance (-1.26 eV [57]), and
- vTi at third-neighbor distance (-0.25 eV [43])

are taken into account, the following four equations must be solved to determine the concentrations of O, Y, and Ti monomers, C_O, C_Y, and C_{Ti}, respectively, and the total vacancy concentration C_v^{total}. These relations correspond to Lomer's equation [58] and are similar to expressions recently published by Schuler *et al.* [3].

The equation for the total vacancy concentration C_v^{total} is

$$C_v^{total} = C_v\{1 - A_v + B_v\}, \tag{13a}$$

with

$$A_v = 6C_O + 8(C_Y + C_{Ti}), \tag{13b}$$

$$B_v = 2\exp\left[-\frac{E^1_{bind}(Ov)}{k_BT}\right]C_O + 4\exp\left[-\frac{E^2_{bind}(Ov)}{k_BT}\right]C_O + 8\exp\left[-\frac{E^3_{bind}(vY)}{k_BT}\right]C_Y + 8\exp\left[-\frac{E^3_{bind}(vTi)}{k_BT}\right]C_{Ti}. \tag{13c}$$

The equation for the total oxygen concentration C_O^{total} is

$$C_O^{total} = C_O\{1 - A_O + B_O\}, \tag{14a}$$

with

$$A_O = 6C_v + 12C_Y + 6C_{Ti}, \tag{14b}$$

$$B_O = 2\exp\left[-\frac{E^1_{bind}(Ov)}{k_BT}\right]C_v + 4\exp\left[-\frac{E^2_{bind}(Ov)}{k_BT}\right]C_v + 4\exp\left[-\frac{E^2_{bind}(OY)}{k_BT}\right]C_Y + 8\exp\left[-\frac{E^5_{bind}(OY)}{k_BT}\right]C_Y + 2\exp\left[-\frac{E^1_{bind}(OTi)}{k_BT}\right]C_{Ti} + 4\exp\left[-\frac{E^2_{bind}(OTi)}{k_BT}\right]C_{Ti}. \tag{14c}$$

The equation for the total Y concentration C_Y^{total} is

$$C_Y^{total} = C_Y\{1 - A_Y + B_Y\}, \tag{15a}$$

with

$$A_Y = 12C_O + 8C_v, \tag{15b}$$

$$B_Y = 4\exp\left[-\frac{E^2_{bind}(OY)}{k_BT}\right]C_O + 8\exp\left[-\frac{E^5_{bind}(OY)}{k_BT}\right]C_O + 8\exp\left[-\frac{E^3_{bind}(vY)}{k_BT}\right]C_v. \tag{15c}$$

The equation for the total Ti concentration C_{Ti}^{total} is

$$C_{Ti}^{total} = C_{Ti}\{1 - A_{Ti} + B_{Ti}\}, \tag{16a}$$

with

$$A_{Ti} = 6C_O + 8C_v, \tag{16b}$$

$$B_{Ti} = 2\exp\left[-\frac{E^1_{bind}(OTi)}{k_BT}\right]C_O + 4\exp\left[-\frac{E^2_{bind}(OTi)}{k_BT}\right]C_O + 8\exp\left[-\frac{E^3_{bind}(vTi)}{k_BT}\right]C_v. \tag{16c}$$

$E^3_{bind}(vY)$ and $E^3_{bind}(vTi)$ denote binding energies at the first-neighbor distance of the bcc lattice which corresponds to the third-neighbor distance in the underlying simple cubic lattice (see Sec. II A). Note that in bcc Fe the interaction between Y and Ti is repulsive and is therefore not considered in Eqs. (13)–(16) [59]. In these equations, the quantity B times the corresponding monomer concentration characterizes the concentration of the considered species (O, v, Y, Ti) within pairs. The quantity $1 - A$ times the corresponding monomer concentration characterizes the concentration of the species which are not in pairs.

It must be mentioned that the thermodynamic approach given in Eqs. (13)–(16) can be considered as a cluster expansion truncated after the pair term. A more general method which allows the consideration of a larger cluster was developed recently by other authors [3,25,60].

In the thermal equilibrium the concentration of single vacancies (monomers) is given by

$$C_v = \exp\left(\frac{-E_F^f}{k_BT}\right), \tag{17}$$

if only the vacancy formation energy at the (ferromagnetic) ground state, E_F^f, is taken into account. This is consistent with Eqs. (13)–(16) where ground-state binding energies are used. At elevated temperature the ground-state quantities should be replaced by free formation and binding energies. In the present work only the phonon and magnetic contributions to the free formation energy of the vacancy F^f are considered. According to Schuler *et al.* [3] F^f is determined by

$$F^f(T) = E_P^f + \left(E_F^f - E_P^f\right)M_0(T)^2 - T\left[S_P^f + \left(S_F^f - S_P^f\right)M_0(T)^2\right], \tag{18}$$

where E_F^f, S_F^f and E_P^f, S_P^f are the formation energy and entropy in ferromagnetic and paramagnetic bcc Fe, respectively, with $E_F^f = 2.12$ eV, $E_P^f = 1.98$ eV, $S_F^f \approx 5k_B$, and $S_P^f \approx 4k_B$ [3]. The quantity $M_0(T)$ denotes the reduced magnetization which varies between 1 (ferromagnetic ground state) and 0 (full paramagnetic state). For $M_0(T)$ the experimental data of Crangle and Goodman [61] are used. Using F^f the monomer vacancy concentration can be calculated by

$$C_\mathrm{v} = \exp\left(\frac{-F^f}{k_B T}\right). \tag{19}$$

The solutions of Eqs. (13)–(16) with C_v from (17) or (19) are shown in Fig. 9. The temperature dependence of the monomer concentrations and of $C_\mathrm{v}^\mathrm{total}$ is illustrated in Fig. 9(a). The difference between the data for $C_\mathrm{v}^\mathrm{total}$ obtained using C_v from (17) or (19) is significant. In Fig. 9(b) the ratios $C_\mathrm{v}/C_\mathrm{v}^\mathrm{total}$, $C_\mathrm{v}^\mathrm{total}/C_\mathrm{O}^\mathrm{total}$, $C_\mathrm{O}/C_\mathrm{O}^\mathrm{total}$, $C_\mathrm{Y}/C_\mathrm{Y}^\mathrm{total}$, and $C_\mathrm{Ti}/C_\mathrm{Ti}^\mathrm{total}$ are depicted. This figure clearly shows that most of the vacancies and most of the O and Y atoms are bound in the corresponding pairs. At very high temperature the values of $C_\mathrm{v}/C_\mathrm{v}^\mathrm{total}$, $C_\mathrm{O}/C_\mathrm{O}^\mathrm{total}$, and $C_\mathrm{Y}/C_\mathrm{Y}^\mathrm{total}$ obtained using C_v from Eq. (19) deviate from those calculated using C_v from Eq. (17) [difference between dashed and solid lines in Fig. 9(b)]. However, these temperatures are not of practical relevance for the thermal processing of ODS alloys. At lower temperature the three ratios show an increase. Furthermore, $C_\mathrm{Ti}/C_\mathrm{Ti}^\mathrm{total}$ is close to 1, which means that most of the Ti atoms are not bound in pairs. This is due to fact that $C_\mathrm{Ti}^\mathrm{total}$ is higher than $C_\mathrm{O}^\mathrm{total}$, $C_\mathrm{Y}^\mathrm{total}$, and $C_\mathrm{v}^\mathrm{total}$, and that the attraction between Ti and the other species is relatively weak. The ratios $C_\mathrm{v}^\mathrm{total}/C_\mathrm{O}^\mathrm{total}$ calculated using C_v from Eqs. (17) or (19) are very different since C_v determined by Eq. (19) is significantly higher. However, in both cases the ratio is much less than 1. This does not agree with the assumption made by several authors [62–64] that in the production of ODS alloys the total vacancy concentration can reach the same order of magnitude as the total concentration of oxygen. On the other hand, it must be emphasized that the data of Fig. 9 were determined under the assumption of the equilibrium between monomers and pairs. Including larger clusters containing O, vacancies, Y, and Ti (see, e.g., [65]) may change the ratio $C_\mathrm{v}^\mathrm{total}/C_\mathrm{O}^\mathrm{total}$ and the other results. In this case equations similar to (13c)–(16c) would contain additional terms with concentrations of the clusters and binding energies of the monomers to the cluster. Furthermore, it must be noticed that the above considerations assume a compact Fe-based material containing a given amount of foreign atoms, and the total vacancy concentration is established by the thermal equilibrium. In reality, at the beginning of the thermal treatment of ODS alloys the material is not compact but more similar to a powder. Therefore, there are certainly additional sources of vacancies so that their concentration should be higher than in a compact material. Thus the data depicted in Fig. 9(b) should be regarded as a lower limit for $C_\mathrm{v}^\mathrm{total}/C_\mathrm{O}^\mathrm{total}$.

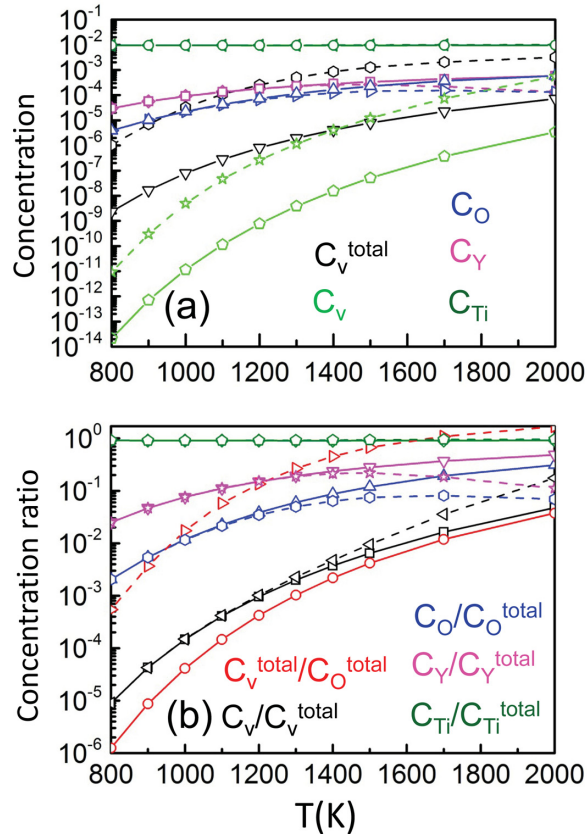

FIG. 9. Temperature dependence of monomer concentrations C_v, C_O, C_Y, C_Ti, and of the total vacancy concentration $C_\mathrm{v}^\mathrm{total}$ (a) as well as the concentration ratios vs temperature (b). The data were obtained by the solution of Eqs. (13)–(16), for the following total concentrations of solutes: 0.18 at.% O, 0.12 at.% Y, and 1.05 at.% Ti. The solid and dashed lines were determined using C_v from Eqs. (17) and (19), respectively.

In the following the diffusion coefficient of oxygen is calculated for the dilute iron alloy using (i) the monomer concentrations C_v, C_Y, and C_Ti shown in Fig. 9(a), or (ii) the total concentrations $C_\mathrm{v}^\mathrm{total}$, $C_\mathrm{Y}^\mathrm{total}$, and $C_\mathrm{Ti}^\mathrm{total}$ given in the above text or depicted in Fig. 9(a) ($C_\mathrm{v}^\mathrm{total}$). The reason why total concentrations are considered is discussed below.

The oxygen diffusion coefficient is determined using expressions similar to Eqs. (8) and (10), but considering interactions not only with v but also with Y and Ti:

$$D = \frac{t_\mathrm{free}}{t_\mathrm{total}}D_\mathrm{free} + \frac{t_\mathrm{inter,v}}{t_\mathrm{total}}D_\mathrm{inter,v} + \frac{t_\mathrm{inter,Y}}{t_\mathrm{total}}D_\mathrm{inter,Y} + \frac{t_\mathrm{inter,Ti}}{t_\mathrm{total}}D_\mathrm{inter,Ti}, \tag{20a}$$

$$t_\mathrm{total} = t_\mathrm{free} + t_\mathrm{inter,v} + t_\mathrm{inter,Y} + t_\mathrm{inter,Ti}, \tag{20b}$$

and

$$\frac{t_{\text{free}}}{t_{\text{total}}} = \frac{1-R_1}{R}, \tag{21a}$$

$$\frac{t_{\text{inter,v}}}{t_{\text{total}}} = \frac{\sum_i N_i \exp\left[-\frac{E^i_{\text{bind}}(\text{Ov})}{k_B T}\right] C^*_{\text{v}}}{R}, \tag{21b}$$

$$\frac{t_{\text{inter,Y}}}{t_{\text{total}}} = \frac{\sum_j N_j \exp\left[-\frac{E^j_{\text{bind}}(\text{OY})}{k_B T}\right] C^*_{\text{Y}}}{R}, \tag{21c}$$

$$\frac{t_{\text{inter,Ti}}}{t_{\text{total}}} = \frac{\sum_k N_k \exp\left[-\frac{E^k_{\text{bind}}(\text{OTi})}{k_B T}\right] C^*_{\text{Ti}}}{R}, \tag{21d}$$

$$R_1 = \sum_i N_i C^*_{\text{v}} + \sum_j N_j C^*_{\text{Y}} + \sum_k N_k C^*_{\text{Ti}}, \tag{21e}$$

$$R_2 = \sum_i N_i \exp\left[-\frac{E^i_{\text{bind}}(\text{Ov})}{k_B T}\right] C^*_{\text{v}} + \sum_j N_j \exp\left[-\frac{E^j_{\text{bind}}(\text{OY})}{k_B T}\right] C^*_{\text{Y}} + \sum_k N_k \exp\left[-\frac{E^k_{\text{bind}}(\text{OTi})}{k_B T}\right] C^*_{\text{Ti}}, \tag{21f}$$

$$R = 1 - R_1 + R_2. \tag{21g}$$

The data for $D_{\text{inter,Y}}$ and $D_{\text{inter,Ti}}$ are calculated by AKMC simulations similarly to the determination of $D_{\text{inter,v}}$; see Sec. III A. As in the determination of concentrations by Eqs. (13)–(19), only the most attractive O-v, O-Y, and O-Ti interactions are taken into account in Eq. (21). The star superscript indicates that monomer or total concentrations are used in two separate types of calculations as already mentioned above. At first the diffusion coefficient is determined using the monomer concentrations C_{v}, C_Y, and C_{Ti}. In reality the diffusion of oxygen may be not only influenced by the v, Y, and Ti monomers but also by pairs or larger clusters which may contain v, Y, or Ti. In a very simple approximation the total concentrations $C^{\text{total}}_{\text{v}}$, $C^{\text{total}}_{\text{Y}}$, and $C^{\text{total}}_{\text{Ti}}$ may be used instead of the monomer concentrations. This is not quite correct since neither the binding energy of an oxygen atom with pairs or larger clusters nor the migration barriers of oxygen in their environment is equal to those in the case of monomers. On the other hand, the calculation of the corresponding binding energies and migration barriers by DFT is an extensive task since many different cluster configurations must be considered. In order to get an idea about the influence of the cluster calculations are therefore performed using $C^{\text{total}}_{\text{v}}$, $C^{\text{total}}_{\text{Y}}$, and $C^{\text{total}}_{\text{Ti}}$.

Figure 10(a) depicts the results for the O diffusion. If only the monomer concentrations C_{v}, C_{Y}, and C_{Ti} are taken into account the diffusion coefficient is already significantly lower than that in pure Fe. The use of either Eq. (17) or Eq. (19) for C_{v} affects the result only at very high temperatures which are not of practical relevance. Below the bcc-to-fcc transition temperature of 1183 K the effective diffusion activation energy is about 1.1 eV. On the other hand, the use of total concentrations $C^{\text{total}}_{\text{v}}$, $C^{\text{total}}_{\text{Y}}$, and $C^{\text{total}}_{\text{Ti}}$ in Eq. (21) leads to an O diffusion coefficient which is still lower than that obtained by considering the monomer concentrations. A large difference is obtained between the results determined using C_{v} from

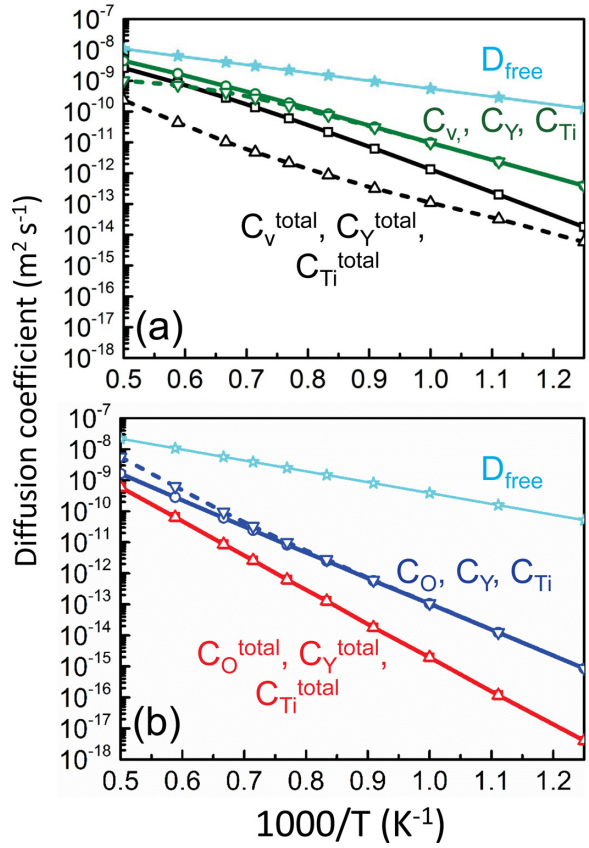

FIG. 10. Total diffusion coefficients of O (a) and v (b) determined for the monomer or the total concentrations shown in Fig. 9(a) and given in the text. The concentrations used in the calculations are written close to the corresponding curves for the diffusion coefficient using the same color. These curves were either obtained using C_{v} from Eq. (17) (solid lines) or C_{v} from Eq. (19) (dashed lines).

Eq. (17) or Eq. (19). The latter case leads to the lowest oxygen diffusion coefficient. This can be explained by the fact that $C^{\text{total}}_{\text{v}}$ is significantly higher than C_{v} [see Fig. 9(a)]. With C_{v} from Eq. (17) or Eq. (19) the diffusion activation energy is about 1.5 or 1.0 eV, respectively, in the temperature range of bcc Fe. The influence of the substitutional foreign atoms on the O diffusion coefficient becomes obvious by comparing with data shown in Fig. 5 of Ref. [2], and in Fig. 6(a), and by considering the concentrations shown in Fig. 9(a): For example, at low temperature the black dashed curve in Fig. 10(a) should be determined by the total concentration of Y (0.12 at. %) and/or Ti (1.05 at. %) since the total v concentration is extremely low. Comparison with diagrams shown in Figs. 5(e) and 5(i) of Ref. [2] clearly shows that the Y content dominates the value of the O diffusion coefficient at temperatures around 800 K. On the other hand, at temperatures near 2000 K the v content is on the order of some tenth of a percent [black dashed line in Fig. 9(a)] and therefore determines the value of the O diffusion coefficient, as one can see by comparing with Fig. 6(a). A similar discussion could be performed concerning the other curves depicted in Fig. 10(a).

Vacancy diffusion in the alloy containing O, Y, and Ti was treated using a method similar to that employed in the calculation of the oxygen diffusion coefficient. The results are

shown in Fig. 10(b). The following cases were considered: (i) Only the monomer concentrations C_O, C_Y, and C_{Ti} [see Fig. 9(a)] were taken into account. (ii) The (constant) total concentrations C_O^{total}, C_Y^{total}, and C_{Ti}^{total} (data given above) were used. Since the monomer concentrations of O, Y, and Ti determined using either Eq. (17) or (19) for C_v are nearly equal, see Fig. 9(a), the resulting values for v diffusion are also not very different. The corresponding diffusion activation energy is about 1.6 eV (below 1183 K). On the other hand, in the calculation of the v diffusivity for the constant total concentrations of O, Y, and Ti the quantity C_v need not be used at all. In the latter case, at 800 K the v diffusion coefficient is about seven orders of magnitude lower than that in perfect bcc Fe, and the activation energy is about 2.13 eV. The comparison of the red line in Fig. 10(b) with the green curve in Fig. 6(b) reveals that the given total O concentration dominates the v diffusion coefficient over the whole temperature range. Thus the influence of Y and Ti is negligible which is due to the weaker binding between v and Y as well as v and Ti compared to that between v and O. Similarly, the blue curves in Fig. 10(b) should be mainly determined by the monomer O concentration.

V. OXYGEN AND VACANCY DIFFUSION IN bcc Fe WITH AN OXYGEN CONTENT CLOSE TO THE VALUE OF THERMAL SOLUBILITY

The few experimental data on oxygen solubility in bcc Fe were published many years ago [5,8,9] and were derived from measurements and calculations performed in connection with internal oxidation experiments. In the temperature range between 800 and 1043 K the data obtained from the formula of Takada *et al.* [8] differ from those of Frank *et al.* [9] by up to one order of magnitude. The value of Swisher and Turkdogan. [5] lies between these data sets (see Supplemental Material [44]). In the present work the solubility data of Takada *et al.* [8] are used. Furthermore, Murali *et al.* [26] calculated by DFT the free formation energy of oxygen by considering equilibrium between Fe and FeO. In the ferromagnetic temperature range the oxygen concentration obtained from these theoretical investigations is somewhat higher than that of Takada *et al.* [8] (see Supplemental Material [44]).

At first the formalism of Sec. IV is employed. The oxygen solubility is set equal to C_O^{total}, and C_v is calculated by Eq. (19). In this manner the monomer O concentration C_O, the total vacancy concentration C_v^{total}, and other quantities are determined (see Supplemental Material [44]). Since both the oxygen and the vacancy concentration are rather low, Eq. (11) can be employed to determine the oxygen diffusion coefficient. A similar relation is used for the vacancy diffusivity. The results obtained by this method are depicted in Fig. 11. If the monomer vacancy concentration C_v is used to determine the time ratio t_{free}/t_{total} in an expression similar to Eq. (10a), the oxygen diffusion coefficient is lower than that for pure bcc Fe but shows a relatively weak temperature dependence [Fig. 11(a)]. This is due to the fact that the value of the free formation energy of the vacancy according to Eq. (18) is not very different from the absolute value of the binding energy of the Ov pair. This may lead to a slight increase of the time ratio t_{free}/t_{total} with decreasing temperature while D_{free} decreases. This peculiarity does not happen if the total vacancy concentration C_v^{total} is used instead of C_v. In this case the oxygen diffusion coefficient is somewhat more similar to the measured data although significant differences remain. The motivation for using the total instead of monomer concentrations was discussed in Sec. IV. On the other hand, Fig. 11(a) clearly shows the discrepancy between the experimental data of Swisher and Turkdogan [5] and Takada *et al.* [6–8]. This underlines the need for further experimental diffusion data directly obtained from an oxygen concentration profile in a sufficiently pure and defect-free bcc Fe. Using the preexponential factor from Eq. (9) and the diffusion activation energy of Frank *et al.* [9] (0.98 eV) another "quasiexperimental" data set was obtained [see Fig. 11(a)].

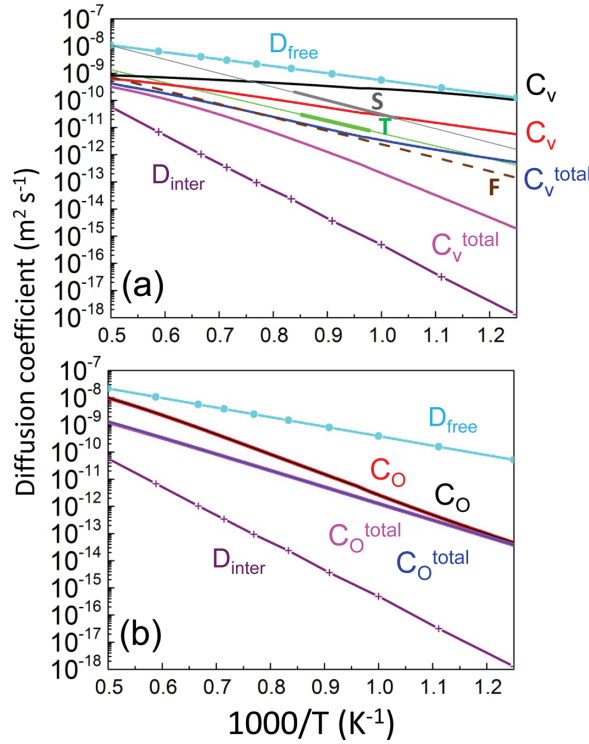

FIG. 11. Total diffusion coefficients of O (a) and v (b) for the case that the oxygen concentration is equal to the thermal solubility. The black and blue curves were determined using monomer and total concentrations, respectively, for O and v. These concentrations were calculated by the method described in Sec. IV. The red and magenta curves were obtained by a modified procedure where not only the O-v interaction (as in Sec. IV) but also the O-Ov (or v-Ov) interactions are taken into account (see Supplemental Material [44]). The red and magenta curves were calculated for monomer and total v or O concentrations, respectively. Note that in (b) the blue and the magenta curves as well as the black and red curves are nearly identical. The oxygen diffusion data determined by internal oxidation experiments are marked by S [5], T [6–8], and F [9]. In the case of S and T the thick lines show the temperature range in which the measurements were performed. Note that the data of Swisher and Turkdogan [5] are based on permeability measurements for δ-iron [4] and are therefore only approximately valid for bcc Fe. The brown dashed line was obtained using the activation energy given by Frank *et al.* [9] and the preexponential factor from Eq. (9).

Schuler *et al.* [3] demonstrated that in the case of bcc Fe with an oxygen content equal to the thermal solubility, not only the Ov pair but also O_2v are important in the determination of the total vacancy concentration. Following Ref. [3] in the present work the formalism of Sec. IV was extended so that not only Ov, but also O_2v and Ov_2 are considered (see Supplemental Material [44]), with binding energies $E_{\text{bind}}^{\text{O2v}} = -3.349\,\text{eV}$ and $E_{\text{bind}}^{\text{Ov2}} = -2.502\,\text{eV}$. That means it is assumed that during O migration not only the Ov pair but also the O_2v cluster may be formed temporarily. Similar to the case without O_2v, calculations were performed assuming C_v or C_v^{total} for the vacancy concentration. In both cases the diffusion activation energy which determines the slope of the curves [red and magenta curves in Fig. 11(a)] is higher than for the respective curves obtained without considering O_2v. Figure 11(b) shows the vacancy diffusion coefficient under the influence of oxygen. Assuming the monomer concentration C_O in the relation for the time ratio $t_{\text{free}}/t_{\text{total}}$ leads to a somewhat higher diffusion activation energy than using C_O^{total}. In both cases the vacancy diffusion coefficient is much lower than that in pure bcc Fe. Taking into account that during v migration not only Ov but also Ov_2 may be formed temporarily does not change the results since in thermal equilibrium the concentration of Ov_2 is very small (see Supplemental Material [44]).

The results presented in this section demonstrate that the presence of a very small amount of oxygen, in the order of the thermal solubility, has a significant influence on both O and v diffusion.

VI. SUMMARY AND CONCLUSIONS

The mutual dependence of O and v diffusion in bcc Fe and dilute iron alloys was investigated using a combined computational method. DFT calculations of the binding energy between O and v at different distances and of the migration barriers of O and v in the regions of their interaction revealed significant special features. The findings of an extremely strong binding of the Ov pair at the first-neighbor distance and of the very high barrier to be overcome for leaving this state are consistent with previous work. On the other hand, it was shown that the Ov pair at the sixth-neighbor distance is instable. This would lower the number of possible migration paths for O and v in the interaction region. However, this reduction is compensated by the simultaneous or coupled jumps of O and v. Furthermore, the investigations showed that a direct v jump from the second- to the fifth-neighbor distance to O is not possible. Ultimately, these peculiarities are due to the very strong attractive interaction of the Ov pair at the first-neighbor state. The DFT results were used as inputs for AKMC-based calculations of the diffusion coefficients of O and v. The consideration of a model system with fixed v or O concentrations already demonstrated the strong influence of vacancies on O diffusion and of oxygen on v diffusion, leading to a significant decrease of the corresponding diffusion coefficients, even if the concentrations are only on the order of some parts per million (ppm). As a more realistic case, the diffusion of O and v during the first stage of thermal processing of ODS alloys was investigated. This system contains ODS-typical total concentrations of O, Y, and Ti. In a simple model thermal equilibrium between O, v, Y, and Ti monomers on the one hand and Ov, OY, OTi, vY, and vTi pairs on the other hand was assumed. Then the O, Y, and Ti monomer concentrations as well as the total v concentration were determined. The O diffusion coefficients obtained for monomer or total concentrations show a significant dependence on the vacancy and the Y content, whereas the v diffusivity is only influenced by the presence of oxygen. Furthermore, a system with an O content close to the thermal solubility in iron was studied. The monomer O concentration as well as the total v concentration was determined using two different models considering equilibrium of O and v with Ov, or equilibrium of O and v with Ov and O_2v or Ov_2. Despite the very small value of thermal solubility of O in bcc Fe, both the O and v diffusion coefficient are very different from that in pure iron. These findings also show that not only the total v concentration or the effective v formation energy is strongly affected by the very small O content, as found by Schuler *et al.* [3], but also the diffusion coefficients of v and O and the corresponding effective diffusion activation energies. The results of the present work have important consequences for planning and performing experiments on O and v diffusion in dilute iron alloys. In particular, a very precise knowledge of the concentrations of O and v, as well as of other foreign atoms and traps such as dislocations, is required. It is also recommended to use bcc Fe single crystals in order to avoid the influence of grain boundaries in such fundamental experiments. The results of the present work are comprehensive and contribute to a better understanding of the interplay between different atomic species and defects in complex materials.

ACKNOWLEDGMENTS

The work of X.W. was financially supported by the China Scholarship Council (File No. 201606240015). The authors thank Dr. Thomas Schuler (CEA, France) for explanation of the formalism of low-temperature expansion (LTE) and Dr. Luca Messina (CEA, France and KTH, Sweden) for providing diffusion data for comparison between results obtained by his method with those determined by our calculations (see Supplemental Material [44]). The authors are grateful to the Center for Information Services and High Performance Computing (ZIH) at Technische Universität Dresden and to the Department of Information Service and Computing at Helmholtz-Zentrum Dresden-Rossendorf for providing extensive computing time. The work also contributes to the Joint Programme on Nuclear Materials (JPNM) of the European Energy Research Alliance (EERA).

[1] H. Mehrer, *Diffusion in Solids*, Springer Series in Solid State Science Vol. 155 (Springer Science & Business Media, Berlin, 2007).

[2] X. Wang, M. Posselt, and J. Faßbender, Influence of substitutional atoms on the diffusion of oxygen in dilute iron alloys, Phys. Rev. B **98**, 064103 (2018).

[3] T. Schuler, C. Barouh, M. Nastar, and C. C. Fu, Equilibrium Vacancy Concentration Driven by Undetectable Impurities, Phys. Rev. Lett. **115**, 015501 (2015).

[4] M. T. Hepworth, R. P. Smith, and E. T. Turkdogan, Permeabiity, solubility, and diffusion of oxygen in bcc iron, Trans. Metall. Soc. AIME **236**, 1278 (1966).

[5] J. H. Swisher and E. T. Turkdogan, Solubility, permeability, and diffusivity of oxygen in solid iron, Trans. Metall. Soc. AIME **239**, 426 (1967).

[6] J. Takada and M. Adachi, Determination of diffusion coefficient of oxygen in α-iron from internal oxidation measurements in Fe-Si alloys, J. Mater. Sci. **21**, 2133 (1986).

[7] J. Takada, S. Yamamoto, S. Kikuchi, and M. Adachi, Internal oxidation of Fe-Al alloys in the α-phase region, Oxid. Met. **25**, 93 (1986).

[8] J. Takada, S. Yamamoto, and M. Adachi, Diffusion coefficient of oxygen in α-iron determined by internal oxidation technique, Z. Metallkd. **77**, 6 (1986).

[9] W. Frank, H. J. Engell, and A. Seeger, Wanderungsenergie und Löslichkeit von Sauerstoff in kubisch raumzentriertem Eisen, Z. Metallkd. **58**, 452 (1967).

[10] C. Barouh, T. Schuler, C. C. Fu, and T. Jourdan, Predicting vacancy-mediated diffusion of interstitial solutes in α-Fe, Phys. Rev. B **92**, 104102 (2015).

[11] S. L. Shang, H. Z. Fang, J. Wang, C. P. Guo, Y. Wang, P. D. Jablonski, Y. Du, and Z. K. Liu, Vacancy mechanism of oxygen diffusivity in bcc Fe: A first-principles study, Corros. Sci. **83**, 94 (2014).

[12] X. Wang, J. Fassbender, and M. Posselt, Efficient calculation methods for the diffusion coefficient of interstitial solutes in dilute alloys, Materials **12**, 1491 (2019).

[13] G. Kresse and J. Hafner, *Ab initio* molecular dynamics for liquid metals, Phys. Rev. B **47**, 558(R) (1993).

[14] G. Kresse and J. Furthmüller, Efficient iterative schemes for *ab initio* total-energy calculations using a plane-wave basis set, Phys. Rev. B **54**, 11169 (1996).

[15] G. Kresse and J. Furthmüller, Efficiency of *ab-initio* total energy calculations for metals and semiconductors using a plane-wave basis set, Comput. Mater. Sci. **6**, 15 (1996).

[16] P. E. Blöchl, Projector augmented-wave method, Phys. Rev. B **50**, 17953 (1994).

[17] G. Kresse and D. Joubert, From ultrasoft pseudopotentials to the projector augmented-wave method, Phys. Rev. B **59**, 1758 (1999).

[18] J. P. Perdew, K. Burke, and M. Ernzerhof, Generalized Gradient Approximation Made Simple, Phys. Rev. Lett. **77**, 3865 (1996).

[19] H. J. Monkhorst and J. D. Pack, Special points for Brillouin-zone integrations, Phys. Rev. B **13**, 5188 (1976).

[20] M. Methfessel and A. T. Paxton, High-precision sampling for Brillouin-zone integration in metals, Phys. Rev. B **40**, 3616 (1989).

[21] C. L. Fu, M. Krcmar, G. S. Painter, and X. Q. Chen, Vacancy Mechanism of High Oxygen Solubility and Nucleation of Stable Oxygen-Enriched Clusters in Fe, Phys. Rev. Lett. **99**, 225502 (2007).

[22] D. Murali, B. K. Panigrahi, M. C. Valsakumar, S. Chandra, C. S. Sundar, and B. Raj, The role of minor alloying elements on the stability and dispersion of yttria nanoclusters in nanostructured ferritic alloys: An *ab initio* study, J. Nucl. Mater. **403**, 113 (2010).

[23] A. Claisse and P. Olsson, First-principles calculations of (Y, Ti, O) cluster formation in body centred cubic iron-chromium, Nucl. Instrum. Methods Phys. Res., Sect. B **303**, 18 (2013).

[24] Y. Jiang, J. R. Smith, and G. R. Odette, Formation of Y-Ti-O nanoclusters in nanostructured ferritic alloys: A first-principles study, Phys. Rev. B **79**, 064103 (2009).

[25] C. Barouh, T. Schuler, C. C. Fu, and M. Nastar, Interaction between vacancies and interstitial solutes (C, N, and O) in α-Fe: From electronic structure to thermodynamics, Phys. Rev. B **90**, 054112 (2014).

[26] D. Murali, M. Posselt, and M. Schiwarth, First-principles calculation of defect free energies: General aspects illustrated in the case of bcc Fe, Phys. Rev. B **92**, 064103 (2015).

[27] H. Jonsson, G. Mills, and K. W. Jacobsen, *Classical and Quantum Dynamics in Condensed Phase Simulations* (World Scientific, Singapore, 1998), pp. 389–404.

[28] G. Henkelman and H. Jonsson, Improved tangent estimate in the nudged elastic band method for finding minimum energy paths and saddle points, J. Chem. Phys. **113**, 9978 (2000).

[29] G. Henkelman, B. P. Uberuaga, and H. Jonsson, A climbing image nudged elastic band method for finding saddle points and minimum energy paths, J. Chem. Phys. **113**, 9901 (2000).

[30] D. Sheppard, P. Xiao, W. Chemelewski, D. D. Johnson, and G. Henkelman, A generalized solid-state nudged elastic band method, J. Chem. Phys. **136**, 074103 (2012).

[31] http://theory.cm.utexas.edu/vtsttools.

[32] L. T. Kong and L. J. Lewis, Transition state theory of the preexponential factors for self-diffusion on Cu, Ag, and Ni surfaces, Phys. Rev. B **74**, 073412 (2006).

[33] G. H. Vineyard, Frequency factors and isotope effects in solid state rate processes, J. Phys. Chem. Solids **3**, 121 (1957).

[34] S. Y. Huang, D. L. Worthington, M. Asta, V. Ozolins, G. Ghosh, and P. K. Liaw, Calculation of impurity diffusivities in α-Fe using first-principles methods, Acta Mater. **58**, 1982 (2010).

[35] C. Wolverton, V. Ozolins, and M. Asta, Hydrogen in aluminum: First-principles calculations of structure and thermodynamics, Phys. Rev. B **69**, 144109 (2004).

[36] A. van de Walle and G. Ceder, The effect of lattice vibrations on substitutional alloy thermodynamics, Rev. Mod. Phys. **74**, 11 (2002).

[37] A. J. Samin, D. A. Andersson, E. F. Holby, and B. P. Uberuaga, *Ab initio* based examination of the kinetics and thermodynamics of oxygen in Fe-Cr alloys, Phys. Rev. B **99**, 174202 (2019).

[38] C. Domain and C. S. Becquart, *Ab initio* calculations of defects in Fe and dilute Fe-Cu alloys, Phys. Rev. B **65**, 024103 (2001).

[39] S. Choudhury, L. Barnard, J. D. Tucker, T. R. Allen, B. D. Wirth, M. Asta, and D. Morgan, *Ab-initio* based modeling of diffusion in dilute bcc Fe–Ni and Fe–Cr alloys and implications for radiation induced segregation, J. Nucl. Mater. **411**, 1 (2011).

[40] H. Amara, C. C. Fu, F. Soisson, and P. Maugis, Aluminum and vacancies in α-iron: Dissolution, diffusion, and clustering, Phys. Rev. B **81**, 174101 (2010).

[41] K. L. Wong, H.-J. Lee, J.-H. Shim, B. Sadigh, and B. D. Wirth, Multiscale modeling of point defect interactions in Fe–Cr alloys, J. Nucl. Mater. **386–388**, 227 (2009).

[42] C. C. Fu, J. Dalla Torre, F. Willaime, J. L. Bocquet, and A. Barbu, Multiscale modelling of defect kinetics in irradiated iron, Nat. Mater. **4**, 68 (2004).

[43] L. Messina, M. Nastar, N. Sandberg, and P. Olsson, Systematic electronic-structure investigation of substitutional impurity diffusion and flux coupling in bcc iron, Phys. Rev. B **93**, 184302 (2016).

[44] See Supplemental Material at http://link.aps.org/supplemental/10.1103/PhysRevB.101.174107 for details on methods and data used in Sec. V.

[45] T. Schuler and M. Nastar, Transport properties of dilute α-Fe(X) solid solutions (X = C, N, O), Phys. Rev. B **93**, 224101 (2016).

[46] T. Schuler, L. Messina, and M. Nastar, KineCluE: A kinetic cluster expansion code to compute transport coefficients beyond the dilute limit, Comput. Mater. Sci. **172**, 109191 (2020).

[47] T. Schuler, M. Nastar, and L. Messina, Mass-transport properties of ternary Fe(C,O) alloys revealed by multicomponent cluster synergies, Phys. Rev. Mater. **4**, 020401(R) (2020).

[48] G. R. Odette, On the status and prospects for nanostrucutred ferritic alloys for nuclear fission and fusion applications with emphasis on the underlying science, Scr. Mater. **143**, 142 (2018).

[49] M. J. Alinger, G. R. Odette, and D. T. Hoelzer, On the role of alloy composition and processing parameters in nanocluster formation and dispersion strengthening in nanostuctured ferritic alloys, Acta Mater. **57**, 392 (2009).

[50] M. K. Miller, D. T. Hoelzer, E. A. Kenik, and K. F. Russell, Nanometer scale precipitation in ferritic MA/ODS alloy MA957, J. Nucl. Mater. **329–333**, 338 (2004).

[51] H. Sakasegawa, F. Legendre, L. Boulanger, M. Brocq, L. Chaffron, T. Cozzika, J. Malaplate, J. Henry, and Y. de Carlan, Stability of non-stoichiometric clusters in the MA957 ODS ferrtic alloy, J. Nucl. Mater. **417**, 229 (2011).

[52] G. R. Odette, M. J. Alinger, and B. D. Wirth, Recent developments in irradiation-resistant steels, Annu. Rev. Mater. Res. **38**, 471 (2008).

[53] G. R. Odette, Recent progress in developing and qualifying nanostructured ferritic alloys for advanced fission and fusion applications, JOM **66**, 2427 (2014).

[54] C. C. Eiselt, M. Klimenkov, R. Lindau, and A. Möslang, Characteristic results and prospects of the 13Cr-1W-0.3Ti-0.3Y_2O_3 ODS steel, J. Nucl. Mater. **386–388**, 525 (2009).

[55] P. He, M. Klimenkov, R. Lindau, and A. Möslang, Characterization of precipitates in nano structured 14% Cr ODS alloys for fusion application, J. Nucl. Mater. **428**, 131 (2012).

[56] A. J. London, S. Santra, S. Amirthapandian, B. K. Panigrahi, R. M. Sarguna, S. Balaji, R. Vijay, C. S. Sundar, S. Lozano-Perez, and C. R. M. Grovenor, Effect of Ti and Cr on dispersion, structure and composition of oxide nano-particles in model ODS alloys, Acta Mater. **97**, 223 (2015).

[57] M. Mock and K. Albe, Diffusion of yttrium in bcc-iron studied by kinetic Monte Carlo Simulations, J. Nucl. Mater. **494**, 157 (2017).

[58] W. M. Lomer, in *Vacancies and Other Point Defects in Metals and Alloys* (Institute of Metals, London, 1958), pp. 79–98.

[59] M. Posselt, D. Murali, and B. K. Panigrahi, Energetics, structure and composition of nanoclusters in oxide dispersion strengthened Fe–Cr alloys, Modell. Simul. Mater. Sci. Eng. **22**, 085003 (2014).

[60] T. Schuler, M. Nastar, and F. Soisson, Vacancy-induced dissolution of precipitates in out-of-equilibrium systems: A test case of FeX (X = C,N,O) alloys, Phys. Rev. B **95**, 014113 (2016).

[61] J. Crangle and G. M. Goodman, The magnetization of pure iron and nickel, Proc. R. Soc. London, Ser. A **321**, 477 (1971).

[62] M. K. Miller, C. L. Fu, M. Krcmar, D. T. Hoelzer, and C. T. Liu, Vacancies as a constitutive element for the design of nanocluster-strengthened ferritic steels, Front. Mater. Sci. China **3**, 9 (2009).

[63] J. Xu, C. T. Liu, M. K. Miller, and H. Chen, Nanocluster-associated vacancies in nanocluster-strengthened ferritic steel as seen via positron-lifetime spectroscopy, Phys. Rev. B **79**, 020204(R) (2009).

[64] X. L. Wang, C. T. Liu, U. Keiderling, A. D. Stoica, L. Yang, M. K. Miller, C. L. Fu, D. Ma, and K. An, Unusual thermal stability of nano-structured ferritic alloys, J. Alloys Compd. **529**, 96 (2012).

[65] M. Vallinayagam, M. Posselt, and J. Faßbender, Investigation of structural models for O–Y and O–Y–Ti clusters in bcc Fe: A density functional theory study, J. Phys.: Condens. Matter **31**, 095701 (2019).